

Evolution of Band Topology by Competing Band Overlap and Spin-Orbit Coupling: Twin Dirac Cones in Ba_3SnO as a Prototype

Toshikaze Kariyado

*International Center for Materials Nanoarchitectonics,
National Institute for Materials Science, Tsukuba 305-0044, Japan**

Masao Ogata

Department of Physics, the University of Tokyo, Bunkyo, Tokyo 113-0033, Japan

(Dated: July 9, 2018)

We theoretically demonstrate how competition between band inversion and spin-orbit coupling (SOC) results in nontrivial evolution of band topology, taking antiperovskite Ba_3SnO as a prototype material. A key observation is that when the band inversion dominates over SOC, there appear “twin” Dirac cones in the band structure. Due to the twin Dirac cones, the band shows highly peculiar structure in which the upper cone of one of the twin continuously transforms to the lower cone of the other. Interestingly, the relative size of the band inversion and SOC is controlled in this series of antiperovskite A_3EO by substitution of A (Ca, Sr, Ba) and/or E (Sn, Pb) atoms. Analysis of an effective model shows that the emergence of twin Dirac cones is general, which makes our argument a promising starting point for finding a singular band structure induced by the competing band inversion and SOC.

Singularities in band structures give rise to singular and attracting responses of materials [1–5]. Therefore, significant amount of efforts have been paid on finding what kinds of singularities are possible in principle, and on proposing materials to realize the singularities, both in theory and experiments [6–8]. The “standard” singularity is Dirac/Weyl cone [9–13], which is characterized by a linear, or conical dispersion around an isolated gap-closing point in the Brillouin zone. Already a number of materials are confirmed to possess Dirac/Weyl cones, ranging from graphene [14] (two-dimensional) to Cd_3As_2 [15], Na_3Bi [16], and TaAs [17] (three-dimensional), and so on. However, the linear dispersion around the isolated gap-closing point is not the only possible band singularity. The gap-closing point can form a line (typically a loop) in the Brillouin zone rather than an isolated point [18–20]. Also, a dispersion around a gap-closing point can be quadratic rather than linear [21]. Very recently, singularities involving three bands are also discussed [22, 23].

Quite often, the three ingredients, i.e., band inversion, spin-orbit coupling (SOC), and symmetry, play key roles in generating a singular band structure. Roughly speaking, the band inversion means an overlap between two bands with different origin, typically originating from different kinds of orbitals, say s- and p-orbitals, or p- and d-orbitals. Naively, the overlapped bands repel with each other (band anticrossing). However the gap opening due to the band repulsion is sometimes prohibited by some symmetry, leading to singular gap closing points. The SOC, on the other hand, determines which kinds of the band repulsion is allowed, in other words, what kinds of gap-closing points can appear.

In this respect, antiperovskite A_3EO family (A=Ca, Sr, Ba and E=Pb, Sn) is an ideal playground to observe singular band structures [24–26]. The representative ma-

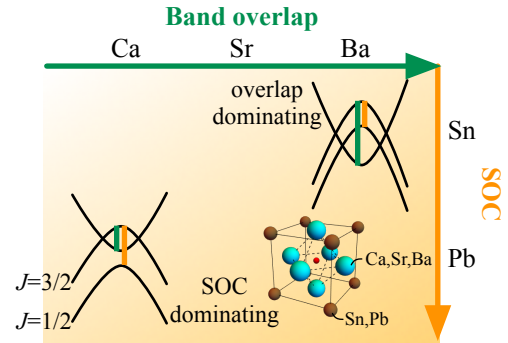


FIG. 1. Schematic description of the evolution of the band topology as a function of the magnitude of the band overlap and the spin-orbit coupling. The crystal structure is shown as inset.

terial Ca_3PbO is predicted to have three-dimensional Dirac cones exactly at the Fermi energy, and importantly, all of the three ingredients, the band overlap, SOC, and the symmetry, are relevant in the formation of Dirac cones. (Strictly speaking, there is a tiny mass gap. If we make an emphasis on the gapful nature, the system is a topological crystalline insulator [27].) It is also worth noting that experiments on this series of materials are now developing. We have highly refined crystal characterization [28], thin film fabrication [29, 30], a thermal measurement [31], and even a report of superconductivity [32].

In this paper, we show that the competition between SOC and the band overlap leads to an interesting evolution of the band structure, taking Ba_3SnO as a prototypical example. In the previous work on the analysis of the antiperovskite family [24], we regarded that the SOC

is dominant, and then, the Dirac cones appear at the Fermi energy as mentioned above. In contrast, we will show that a new kind of band singularity is generated when SOC is smaller than the band inversion. The new singularity involves three (six if we count the spin degrees of freedom) bands, which is similar to Refs. 22 and 23. Specifically, we find “twin” Dirac cones, which have small separation in the energy and momentum space. The upper branch of the lower-energy Dirac cone continuously transforms into the lower branch of the higher-energy Dirac cone, which results in a peculiar evolution of the isoenergy surfaces as a function of the energy. It is worth noting that the size of the band overlap can be controlled by the choice of Ca, Sr, or Ba, while the size of the SOC by the choice of Sn or Pb in A_3EO , namely, we can design the band singularity. (See Fig. 1.) We further propose a simple effective model to extract the essence of this band singularity and show that the emergence of the twin Dirac cones is general. These findings form a concise guideline to search for novel states of matter originating from the competition between SOC and the band overlap.

Let us start with describing the band structure of Ba_3SnO . The first-principles calculation is carried out with Quantum Espresso package [33]. In order to incorporate SOC, the relativistic projector augmented wave (PAW) data sets from pslibrary 1.0.0 are employed [34]. The cutoff energies for the wave function and the charge density are 50 and 400 Ry, respectively. We use the experimental crystal structure, i.e., cubic with the lattice constant $a_0 = 5.448 \text{ \AA}$ [35]. The recent refinement of the crystal structure reveals that the zero temperature structure is slightly distorted from the cubic structure [28]. However, since the symmetry of the crystal plays an important role, we stick with the cubic symmetry realized at room temperature. Strictly speaking, the density functional theory for the first-principles calculation is for zero temperature, but we assume that the essence of the band singularity is safely captured. The effect of the distortion will be briefly discussed at the end.

The obtained band structure is shown in Fig. 2(a). The entangled bands above the Fermi energy stem from d-orbitals (Ba-5d), while the bands right below the Fermi energy from p-orbitals (Sn-5p). An inspection of the orbital character of each band reveals that the top of the p-bands lies above the bottom of the d-bands, i.e., there is an overlap. There are two (twin) Dirac cones in the region marked by a circle on Γ -X line in Fig. 2(a). The singular structure of these twin cones becomes clear in the three-dimensional plots of the dispersion relations shown in Figs. 2(b) and 2(c). For $k_z = 0$ [Fig. 2(b)], we observe two Dirac cone structures with small separation, and we denote the higher and lower energy ones DC1 and DC2, respectively. The upper branch of DC2 is continuously turns into the lower branch of DC1. Figure 2(c) with $k_z = 0.005$ shows that the gap grows as $|k_z|$ increases, which signals the three-dimensional nature of the Dirac

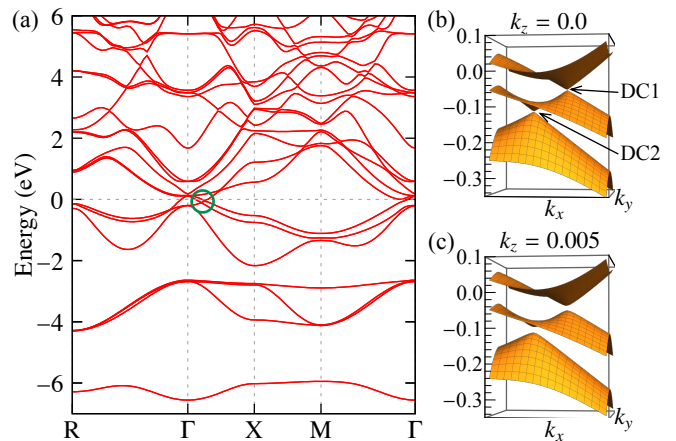


FIG. 2. (Color online) (a) Global band structure of Ba_3SnO . (b,c) Dispersion relations of the three bands relevant to the twin Dirac cones. The plotted region is $0.07 \leq k_x \leq 0.17$ and $-0.05 \leq k_y \leq 0.05$ with $k_z = 0.0$ (b) and $k_z = 0.005$ (c). The momenta are measured in the unit of $2\pi/a_0$, where a_0 represents the lattice constant.

cones. If we look at the band structure closely, it turns out that DC1 has a tiny mass gap (less than 2 meV), while DC2 is exactly gapless. Note that the existence of the two Dirac cones on the Γ -X line implies that there are 12 Dirac cones in the entire Brillouin zone due to the cubic symmetry.

Let us compare Ba_3SnO and Ca_3PbO more in detail in order to elucidate the essence determining the difference in the band topology. As in Fig. 1, these compounds share the same feature of the overlapping d- and p-bands, but the critical difference lies in the magnitude of the band overlap and SOC. We can see this from Fig. 3, where the close-up view of the band structure on Γ -X line is shown with the irreducible representation for each band. Owing to SOC, p-bands are split into $J = 3/2$ and $J = 1/2$ states. At Γ -point, Γ_8^- and Γ_6^- correspond $J = 3/2$ and $J = 1/2$ states, respectively. Therefore, the energy difference between Γ_8^- and Γ_6^- , represented as orange vertical bars in Fig. 3, measures the size of SOC. On the other hand, in the energy range of Fig. 3, the lowest-energy Γ_8^+ state at Γ -point represents the bottom of the d-bands, and thus, the energy difference between the lowest Γ_8^+ and Γ_8^- (green bars in Fig. 3) is regarded as the size of the band overlap. Apparently, the band overlap is larger than SOC in Ba_3SnO , while it is opposite in Ca_3PbO .

Using this difference in the size of SOC and band overlap, the band topologies in Ba_3SnO and Ca_3PbO are explained as follows. By definition, when the band overlap is larger than SOC as in Ba_3SnO , the $J = 1/2$ band is above the bottom of the d-bands at Γ -point, while when SOC is larger than the band overlap as in Ca_3PbO , the $J = 1/2$ band comes below the bottom of the d-bands.

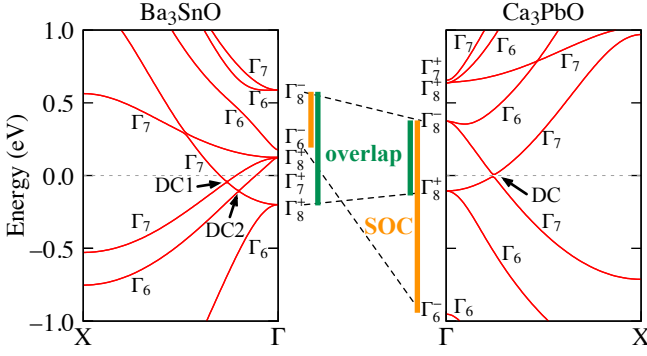


FIG. 3. (Color online) Band structures on the Γ -X line along with the irreducible representations of the bands. The left (right) panel shows the band structure of Ba_3SnO (Ca_3PbO). The Dirac points are marked with arrows.

Then, by following the way in which the bands are connected in Fig. 3, we see that the gap-closing point defined as DC2 is allowed only when the $J = 1/2$ band is above the bottom of the d-bands as in the case of Ba_3SnO . Therefore, two Dirac cones, DC1 and DC2 appear in Ba_3SnO , while only one in Ca_3PbO . Next, the reason for Ba_3SnO having larger band overlap than Ca_3PbO is that the band width of the Ba-5d orbital is larger than that of the Ca-3d orbital, and as a result, the bottom of the Ba-5d band is lower than that of the Ca-3d band. This difference between Ba-5d and Ca-3d originates from the difference of the spreading of the wave functions for Ba-5d and Ca-3d orbitals. On the other hand, SOC in this series of materials is mostly provided by Sn or Pb atoms. Therefore SOC is weaker in Ba_3SnO than Ca_3PbO . To summarize, Ba_3SnO is a band-overlap-dominant material whereas Ca_3PbO is an SOC-dominant material, which explains the difference in the band topology. The argument here suggests that the band topology can be controlled by partial substitution of A and E atoms in A_3EO . (See Fig. 1.)

From Fig. 3, we can also understand the existence and nonexistence of the mass gap at DC1 and DC2. We see that DC1 is a crossing between two Γ_7 bands, while DC2 is a crossing between Γ_6 and Γ_7 . Therefore, DC1 can have finite mass gap in principle. Specifically, the gap at DC1 is induced by the indirect spin-orbit coupling involving the states far away from the Fermi energy as discussed before in Ca_3PbO [24, 25]. Since it involves the far away states, the gap at DC1 is tiny as obtained in the first-principles calculation. In contrast, DC2 is exactly gapless, which is protected by the crystalline symmetry, just as in the case of the known Dirac semimetals like Cd_3As_2 or Na_3Bi .

A highly peculiar band structure associated with the twin Dirac cones becomes apparent if we look at the isoenergy surfaces for several energies, which would represent the doping dependence of the Fermi surfaces in the

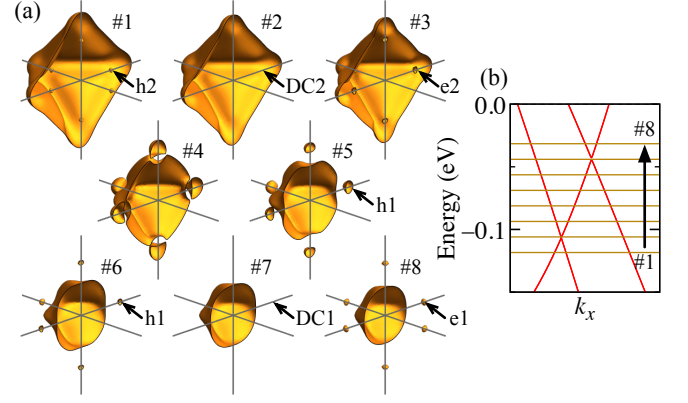


FIG. 4. (Color online) Energy evolution of the isoenergy surfaces of the three bands relevant to the Dirac cones. The selected energy for each surface is represented in (b). In each panel, some part of the isoenergy surface is eliminated to make the inside visible.

rigid-band assumption. Figure 4 shows the isoenergy surfaces for energies #1 -0.1184 , #2 -0.106 , #3 -0.0936 , #4 -0.0812 , #5 -0.0688 , #6 -0.0564 , #7 -0.044 , and #8 -0.0316 in the unit of eV measured from the undoped Fermi energy. [Figure 4(b) shows the selected energies.] In #1, we observe two types of isoenergy surfaces: one is a large surface associated with the non-Dirac hole-like band, and the others are small and almost point-like surfaces [shown as h2 in Fig. 4(a)] associated with the lower branch of DC2 inside of the larger surface. As the energy is increased, i.e. #1 \rightarrow #3, the large hole-like surface gradually shrinks. On the other hand, h2 first shrinks, disappears at #2 (Dirac point of DC2), and reappears as a small surface e2, which is the upper branch of DC2 having electron-like nature. As the energy increases further, e2 expands, and at a certain energy around #4, topology of the isoenergy surfaces changes. After this topological change, e2 turns into h1, which is now hole-like and outside of the larger surface. Then, there appear small hole surfaces (h1) as shown in #5. Since h1 is the lower branch of DC1, it disappears at #7 (Dirac point of DC1) and reappears as a small electron-like surface e1 when the energy is further increased. The discovered topological change of the isoenergy surface must cause interesting doping dependent responses in measurements sensitive to Fermi surface shapes, such as the quantum oscillation.

Next, we show that the emergence of the twin Dirac cones are generic by constructing a minimal effective model. For this purpose, we focus on the band structure along the k_z -axis, on which C_{4v} point-group symmetry is effective. Before taking SOC into account, there are five irreducible representations in C_{4v} : A_1 , A_2 , B_1 , B_2 , and E . Intuitively, s , p_z , and $d_{3z^2-r^2}$ orbitals correspond to A_1 representation, $d_{x^2-y^2}$ orbital to B_1 , d_{xy} orbital to

B_2 , and $p_{x/y}$ and $d_{zx/yz}$ orbitals to E. From the orbital weight analysis of the bands, we find that $p_{x/y}$ orbitals of Sn (or Pb) and $d_{x^2-y^2}$ orbitals of Ba (or Ca, Sr) are responsible for the twin generation. Therefore, we keep the E and B_1 states in the minimal effective model. By adding SOC as $\mathbf{L} \cdot \mathbf{S}$ coupling on the atomic p-orbitals, we obtain the effective Hamiltonian as

$$\hat{H} = \begin{pmatrix} g_p(k_z) & -i\lambda & hk_x & 0 & 0 & 0 \\ i\lambda & g_p(k_z) & -hk_y & 0 & 0 & 0 \\ hk_x & -hk_y & g_d(k_z) & 0 & 0 & 0 \\ 0 & 0 & 0 & g_p(k_z) & i\lambda & hk_x \\ 0 & 0 & 0 & -i\lambda & g_p(k_z) & -hk_y \\ 0 & 0 & 0 & hk_x & -hk_y & g_d(k_z) \end{pmatrix}, \quad (1)$$

where the basis wave functions are $|p_x \uparrow\rangle$, $|p_y \uparrow\rangle$, $|d \uparrow\rangle$, $|p_x \downarrow\rangle$, $|p_y \downarrow\rangle$, $|d \downarrow\rangle$, and λ is the coefficient for SOC. The matrix elements in Eq. (1) are kept up to the first order in k_x and k_y , since we focus on the effective model in the vicinity of k_z -axis. Due to the difference in symmetry between $p_{x/y}$ and $d_{x^2-y^2}$ orbitals, the offdiagonal elements are linear in k_x and k_y .

When we switch to the basis set that diagonalizes SOC, the Hamiltonian Eq. (1) becomes $\hat{H} = \hat{H}_\lambda \oplus \hat{H}_{-\lambda}$ with

$$\hat{H}_\lambda = \begin{pmatrix} g_p(k_z) + \lambda & 0 & hk_- \\ 0 & g_p(k_z) - \lambda & hk_+ \\ hk_+ & hk_- & g_d(k_z) \end{pmatrix}, \quad (2)$$

where $k_\pm \equiv k_x \pm ik_y$. Now, suppose that there exists k_{z0}^\pm satisfying $g_p(k_{z0}^\pm) \pm \lambda = g_d(k_{z0}^\pm)$. Then, near $k_z = k_{z0}^\pm$, $g_p(k_z)$ and $g_d(k_z)$ can be expanded as $g_p(k_z) \pm \lambda = \epsilon_\pm + c_p^\pm(k_z - k_{z0}^\pm)$ and $g_d(k_z) = \epsilon_\pm - c_d^\pm(k_z - k_{z0}^\pm)$. Using this expression, the effective Hamiltonian around $\mathbf{k} = (0, 0, k_{z0}^\pm)$ becomes $\hat{H} = \hat{H}^{(+)} \oplus \hat{H}^{(-)}$ with

$$\hat{H}^{(\pm)} = (\epsilon_\pm + \delta c_\pm \delta k_z^\pm) + \begin{pmatrix} c_\pm \delta k_z^\pm & hk_\mp \\ hk_\pm & -c_\pm \delta k_z^\pm \end{pmatrix}, \quad (3)$$

where $\delta k_z^\pm = k_z - k_{z0}^\pm$, $c_\pm = (c_p^\pm + c_d^\pm)/2$, and $\delta c_\pm = (c_p^\pm - c_d^\pm)/2$. This effective Hamiltonian is nothing more than Dirac Hamiltonian. The parameter δc_\pm in Eq. (3) determines the tilting angle of the Dirac cone, and when the slopes of $g_p(k_z)$ and $g_d(k_z)$ are nearly opposite (i.e., $c_p^\pm \sim c_d^\pm$), this tilting angle becomes small. Note that the state neglected in deriving Eq. (3) from Eq. (2) only affects the resultant model at least in the second order with respect to k_\pm .

The above results are interpreted in the language of the competing band overlap and SOC as follows. Firstly, for the band-overlap dominant case, e.g., in Ba_3SnO , both of the two conditions, $g_p(k_z) + \lambda = g_d(k_z)$ and $g_p(k_z) - \lambda = g_d(k_z)$ can be satisfied, which leads to the twin Dirac cones. On the other hand, for the SOC dominant case, e.g., in Ca_3PbO , only $g_p(k_z) + \lambda = g_d(k_z)$ has a valid solution, while $g_p(k_z) - \lambda = g_d(k_z)$ cannot have a solution at any k_z in the Brillouin zone since λ is large. In this

way, the number of Dirac cones is correctly reproduced in this minimal effective model. It is also worth noting that the twin Dirac cones are merged in the $\lambda = 0$ limit since two conditions $g_p(k_z) \pm \lambda = g_d(k_z)$ become identical. Inversely speaking, the twin cones are generated by SOC. Although the above model is derived with a specific kind of material in mind, the strong restriction is only from the cubic symmetry, and thus, the model can be realized in a wide class of materials. All we have to do is to find a way to control the band-overlap and SOC, which is relatively simple in our A_3EO by partial substitution in A and E atoms.

Before closing, we make a few comments on our theoretical approach. Firstly, we have considered the room temperature cubic structure instead of the zero temperature distorted structure, in order to take advantage of the high symmetry. We have performed some band structure calculation with distortion (not shown). We find that, because of the symmetry reduction, even DC2 becomes gapful, although the gap is small partially because the distortion is still perturbative to the original cubic structure [28]. The second comment is about our computational methods. We have applied a standard density functional theory, but we should note that a precise prediction of the band overlap size is challenging [36]. For example, HSE correction gives different numbers for the size of the overlap [27]. However, the overall tendency is unaltered by some computational details, i.e., the tendency that Ba based compound has a larger band overlap than the Ca based one will not change. Therefore, the essence of the present paper to give a unified view on the band topology due to the competition between SOC and band overlap will be unchanged.

To summarize, the band structure of Ba_3SnO is investigated by means of the first-principles method, and twin Dirac cones and associated peculiar band dispersions are disclosed. Behind this phenomenon, there is a competition between the band overlap and the spin-orbit coupling. Further study on A_3EO (A=Ca, Sr, Ba and E=Sn, Pb) should be worthwhile, since it provides a simple way to control the band overlap and the spin-orbit coupling by chemical substitution. We believe that the concept of competing band overlap and spin-orbit coupling is useful in future exploration of novel states of matter.

The authors thank H. Takagi for stimulating discussions. TK thanks the Supercomputer Center, the Institute for Solid State Physics, the University of Tokyo for the use of the facilities. This work was supported by a Grant-in-Aid for Scientific Research No. 15H02108 (MO) and No. 17K14358 (TK).

* kariyado.toshikaze@nims.go.jp

- [1] H. Fukuyama and R. Kubo, *J. Phys. Soc. Jpn.* **28**, 570 (1970).
- [2] A. H. Castro Neto, F. Guinea, N. M. R. Peres, K. S. Novoselov, and A. K. Geim, *Rev. Mod. Phys.* **81**, 109 (2009).
- [3] A. A. Burkov, *Nat Mater* **15**, 1145 (2016).
- [4] S. Jia, S.-Y. Xu, and M. Z. Hasan, *Nat Mater* **15**, 1140 (2016).
- [5] N. P. Armitage, E. J. Mele, and A. Vishwanath, *arXiv:1705.01111*.
- [6] H. Weng, X. Dai, and Z. Fang, *J. Phys: Condens. Mat.* **28**, 303001 (2016).
- [7] M. Z. Hasan, S.-Y. Xu, I. Belopolski, and S.-M. Huang, *Ann. Rev. Condens. Mat. Phys.* **8**, 289 (2017).
- [8] B. Yan and C. Felser, *Ann. Rev. Condens. Mat. Phys.* **8**, 337 (2017).
- [9] P. R. Wallace, *Phys. Rev.* **71**, 622 (1947).
- [10] X. Wan, A. M. Turner, A. Vishwanath, and S. Y. Savrasov, *Phys. Rev. B* **83**, 205101 (2011).
- [11] A. A. Burkov and L. Balents, *Phys. Rev. Lett.* **107**, 127205 (2011).
- [12] Z. Wang, Y. Sun, X.-Q. Chen, C. Franchini, G. Xu, H. Weng, X. Dai, and Z. Fang, *Phys. Rev. B* **85**, 195320 (2012).
- [13] Z. Wang, H. Weng, Q. Wu, X. Dai, and Z. Fang, *Phys. Rev. B* **88**, 125427 (2013).
- [14] K. S. Novoselov, A. K. Geim, S. V. Morozov, D. Jiang, M. I. Katsnelson, I. V. Grigorieva, S. V. Dubonos, and A. A. Firsov, *Nature* **438**, 197 (2005).
- [15] M. Neupane, S.-Y. Xu, R. Sankar, N. Alidoust, G. Bian, C. Liu, I. Belopolski, T.-R. Chang, H.-T. Jeng, H. Lin, A. Bansil, F. Chou, and M. Z. Hasan, *Nature Commun.* **5**, 3786 EP (2014).
- [16] Z. K. Liu, B. Zhou, Y. Zhang, Z. J. Wang, H. M. Weng, D. Prabhakaran, S.-K. Mo, Z. X. Shen, Z. Fang, X. Dai, Z. Hussain, and Y. L. Chen, *Science* **343**, 864 (2014).
- [17] B. Q. Lv, N. Xu, H. M. Weng, J. Z. Ma, P. Richard, X. C. Huang, L. X. Zhao, G. F. Chen, C. E. Matt, F. Bisti, V. N. Strocov, J. Mesot, Z. Fang, X. Dai, T. Qian, M. Shi, and H. Ding, *Nat Phys* **11**, 724 (2015).
- [18] C. Herring, *Phys. Rev.* **52**, 365 (1937).
- [19] A. A. Burkov, M. D. Hook, and L. Balents, *Phys. Rev. B* **84**, 235126 (2011).
- [20] A. Yamakage, Y. Yamakawa, Y. Tanaka, and Y. Okamoto, *J. Phys. Soc. Jpn.* **85**, 013708 (2016).
- [21] K. Sun, H. Yao, E. Fradkin, and S. A. Kivelson, *Phys. Rev. Lett.* **103**, 046811 (2009).
- [22] B. Q. Lv, Z.-L. Feng, Q.-N. Xu, J.-Z. Ma, L.-Y. Kong, P. Richard, Y.-B. Huang, V. N. Strocov, C. Fang, H.-M. Weng, Y.-G. Shi, T. Qian, and H. Ding, 1610.08877 (2016).
- [23] Z. Zhu, G. W. Winkler, Q. S. Wu, J. Li, and A. A. Soluyanov, *Phys. Rev. X* **6**, 031003 (2016).
- [24] T. Kariyado and M. Ogata, *J. Phys. Soc. Jpn.* **80**, 083704 (2011).
- [25] T. Kariyado and M. Ogata, *J. Phys. Soc. Jpn.* **81**, 064701 (2012).
- [26] M. Klintonberg, J. T. Haraldsen, and A. V. Balatsky, *Appl. Phys. Res.* **6**, 31 (2014).
- [27] T. H. Hsieh, J. Liu, and L. Fu, *Phys. Rev. B* **90**, 081112 (2014).
- [28] J. Nuss, C. Mühle, K. Hayama, V. Abdolazimi, and H. Takagi, *Acta Cryst. B* **71**, 300 (2015).
- [29] Y. F. Lee, F. Wu, R. Kumar, F. Hunte, J. Schwartz, and J. Narayan, *Applied Physics Letters* **103**, 112101 (2013).
- [30] D. Samal, H. Nakamura, and H. Takagi, *APL Materials* **4**, 076101 (2016).
- [31] Y. Okamoto, A. Sakamaki, and K. Takenaka, *J. Appl. Phys.* **119**, 205106 (2016).
- [32] M. Oudah, A. Ikeda, J. N. Hausmann, S. Yonezawa, T. Fukumoto, S. Kobayashi, M. Sato, and Y. Maeno, *Nature Commun.* **7**, 13617 EP (2016).
- [33] P. Giannozzi, S. Baroni, N. Bonini, M. Calandra, R. Car, C. Cavazzoni, D. Ceresoli, G. L. Chiarotti, M. Cococcioni, I. Dabo, A. Dal Corso, S. de Gironcoli, S. Fabris, G. Fratesi, R. Gebauer, U. Gerstmann, C. Gougoussis, A. Kokalj, M. Lazzeri, L. Martin-Samos, N. Marzari, F. Mauri, R. Mazzarello, S. Paolini, A. Pasquarello, L. Paulatto, C. Sbraccia, S. Scandolo, G. Sclauzero, A. P. Seitsonen, A. Smogunov, P. Umari, and R. M. Wentzcovitch, *J. Phys.: Condens. Matter* **21**, 395502 (2009).
- [34] <http://www.quantum-espresso.org/pseudopotentials/pslibrary/>.
- [35] A. Widera and H. Schäfer, *Mater. Res. Bull.* **15**, 1805 (1980).
- [36] J. Vidal, X. Zhang, L. Yu, J.-W. Luo, and A. Zunger, *Phys. Rev. B* **84**, 041109 (2011).